Near-Ultraviolet Luminescence of N_2 Irradiated by Short X-Ray Pulses

Stefan P. Hau-Riege, Richard M. Bionta, Dmitri D. Ryutov, Richard A. London, Elden Ables, Keith I. Kishiyama, Stewart Shen, Mark A. McKernan, and Donn H. McMahon
Lawrence Livermore National Laboratory, 7000 East Avenue, Livermore, California 94550, USA

Marc Messerschmidt, Jacek Krzywinski, Peter Stefan, and James Turner
SLAC National Accelerator Laboratory, 2575 Sand Hill Road, Menlo Park, California 94025, USA

Beata Ziaja
Center for Free-Electron Laser Science, DESY, D-22607 Hamburg, Germany
(Received 7 May 2010; published 23 July 2010)

The Linac Coherent Light Source is an x-ray free-electron laser that recently demonstrated lasing in the 1.5–15 Å wavelength range. We report on luminescence measurements of a molecular nitrogen gas irradiated by ~2 mJ, 80 fs x-ray pulses at energies of 0.83, 2.7, and 8.3 keV. These results provide a direct test of our current understanding of photoabsorption, electron dynamics, and fluorescence processes for such intense, ultrashort x-ray pulses. At 0.83 keV, the duration of the fluorescence signal depends strongly on space-charge effects. At 8.3 keV, space-charge effects are weak, and the signal duration is determined by the Auger electron dynamics.

DOI: 10.1103/PhysRevLett.105.043003 PACS numbers: 33.80.Rv, 07.85.Fv, 41.60.Cr, 52.25.Os

X-ray free-electron lasers (XFELs) are tunable, high-power sources of short pulse photon radiation. The first hard XFEL, the Linac Coherent Light Source (LCLS), has recently become available, producing photon pulses between 0.83 and 8.3 keV, with pulse lengths ranging from 10 to 300 fs and pulse energies up to 4 mJ [1,2]. The revolutionary output characteristics of XFELs propel us into a new regime of x-ray matter interaction. Our Letter presents a first example of a systematic experimental study of a classical problem of x-ray-induced photoluminescence of a gaseous medium, but under conditions of extreme intensities and small beam cross sections typical of LCLS. We find that these new conditions bring new dimensions to the problem, giving rise to nontrivial interplay between atomic physics and collective effects in ensembles of charged particles. In addition to being of general physical interest, this problem is also related to developing new techniques for characterizing XFEL beam parameters. At the LCLS, nitrogen fluorescence is used to measure the individual pulse energies *in situ* with minimal perturbation [3]. Currently, these fluorescence detectors are cross-calibrated using destructive pulse-energy-measurement methods. Our study helps the understanding of the device physics and may ultimately lead to an absolute calibration.

In the usual operation of LCLS, a 0.25 nC electron bunch with a transverse emittance less than 1 μm is injected into the last 1-km-long section of the SLAC linear accelerator. The electron bunch length is reduced using two compressors in the accelerator, and then injected into a 132-m-long undulator consisting of 33 segments. Each segment is a fixed-gap planar-hybrid undulator utilizing NdFeB magnets. The undulator period is 3 cm. The undulator is operated near the FEL collective instability, leading to the emission of high-brightness x-ray pulses that are linearly polarized in the horizontal direction. Our experiments were performed using 0.83, 2.7, and 8.3 keV photons. The pulse energy ranged from 1 to 2 mJ.

The LCLS radiation interacted with the nitrogen gas 80 m downstream from the exit of the undulator. The rms spot diameters of the pulses were approximately 600, 400, and 200 μm at 0.83, 2.7, and 8.3 keV, respectively. The error in the spot size is about 30%. The nitrogen gas was contained in a 30-cm-long vessel that was lined with an 8-cm-diameter cylindrical aluminum insert. The vessel ends had 4 mm orifices through which the chamber was differentially pumped. Figure 1 shows the experimental setup. Photoionization of the gas produces primary, Auger, and secondary electrons, which ultimately produce UV fluorescence of the nitrogen. We used a solenoid to create an axial magnetic field to maximize the residence time of the electrons in the nitrogen gas. The time dependence of the fluorescence signal was detected using two Hamamatsu photomultiplier tubes (PMTs) that were sampled with a 10-bit analog-to-digital converter with a 3 ns temporal resolution. The PMTs were positioned to observe the center of the vessel, pointing parallel and perpendicular to the

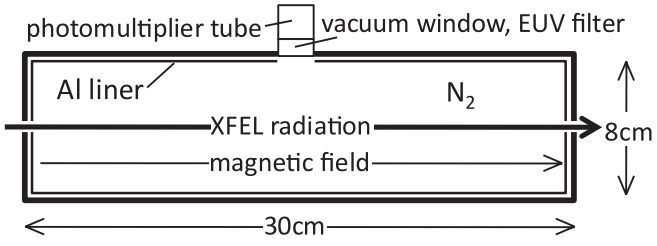

FIG. 1. Experimental setup.

electric field vector of the LCLS pulses. The field of view of the PMTs spanned nearly the full interaction region. A near-UV filter was inserted in front of the PMT that was transparent to light between 300 and 390 nm [3]. At each wavelength, a sufficiently low nitrogen pressure was chosen so that the PMTs did not saturate.

Examples of the temporal dependence of the fluorescence signal for different nitrogen pressures, magnetic fields, and photon energies are shown in Fig. 2. Each of these curves is an average over approximately 50 pulses to improve the signal-to-noise ratio. The fluorescence signals generally show a rapid rise, followed by a slow decay. At larger nitrogen densities, the signals become less noisy since more x-ray photons are absorbed and more UV light is generated. At higher photon energies, larger nitrogen densities are needed to maintain a similar signal level since the photon absorption cross section decreases: Compared to 0.83 keV, the x-ray absorption cross section for N_2 is 28 times smaller at 2.7 keV, and 856 times smaller at 8.3 keV [4]. In certain cases, notably at 0.83 keV and 12 mTorr, a short signal spike occurs with a temporal width of a few nanoseconds. In most other cases, this spike is much less pronounced and can only be discerned as a slight change in the slope of the initial signal. This spike is likely due to fluorescence in the aluminum liner and the vacuum window induced by scattered x-ray photons.

We now discuss the interaction of the short x-ray pulse with the nitrogen gas. In more than 95% of all cases, x-ray photons are absorbed through K-shell photoionization. Next likely is ionization of the outer L shell. Photoexcitation processes at 0.83–8.3 keV are rare. The photoelectron has a kinetic energy of $E_{\text{x-ray}} - E_{\text{ion}}$, where

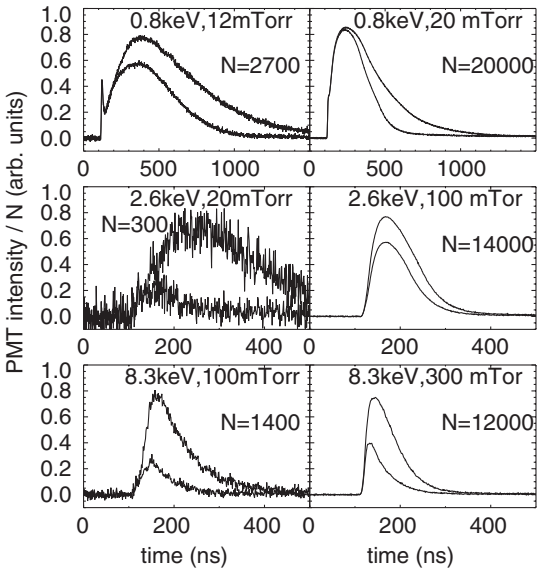

FIG. 2. Temporal dependence of the fluorescence signal for different nitrogen pressures, magnetic fields, and photon energies, measured with the PMT located at the top of the chamber. For the lower and upper curves the magnetic field is 0 and 240 G, respectively. N is the normalization constant.

$E_{\text{x-ray}}$ is the x-ray energy and $E_{\text{ion}} \approx 410$ eV for K-shell ionization. For pulse energies of 2 mJ, the fractions of photoionized molecules are only 1.7×10^{-4}, 4.5×10^{-6}, and 2.0×10^{-7} for photon energies of 0.83, 2.7, and 8.3 keV, respectively, assuming the spot sizes mentioned above. The core-hole-ionized molecules decay primarily through Auger relaxation within a few femtoseconds, leading to the emission of electrons with a kinetic energy of approximately 400 eV. The photoelectrons and Auger electrons interact further with the gas through impact ionization and excitation. The electrons downscatter creating a cascade of low energy secondary electrons. Electron excitation ultimately leads to UV emission and is more probable at lower impact energies ($\leq$30 eV) [5]. In the wavelength regime of 300–390 nm, fluorescence originates from the first negative system of N_2^+ ($B\,^2\Sigma_u^+ \rightarrow X\,^2\Sigma_g^+$) and the second positive system of N_2 ($C\,^3\Pi_u \rightarrow B\,^3\Pi_g$). Only a very small fraction of the electrons that deposit their energy through inelastic collisions produce this fluorescence [6]. The characteristic time scales that determine the fluorescent decay time τ_f are (i) the radiative decay time, which ranges from 10 to 200 μs for the dominant lines, (ii) the lifetime associated with internal quenching of the nitrogen molecules, ranging from 20 to 30 ns, and (iii) the collisional deexcitation lifetime, which ranges from 80 ns to 3 μs for the different fluorescence lines at 1 Torr [7]. The fluorescence decay is therefore dominated by the internal quenching and is approximately 20–30 ns.

For x-ray energies ranging from 0.83 to 8.3 keV, the photoelectrons have velocities ranging from 12 to 54 nm/fs, corresponding to 4%–18% of the velocity of light. During the pulse duration of $\sim$80 fs, the photoelectrons travel only 1–4 μm, which is much smaller than the beam diameter. A 80 fs pulse is 24 μm long and needs approximately 1 ns to traverse the 30-cm-long chamber. Neglecting stopping by the nitrogen molecules, the photoelectrons move 12–54 mm during this time, while the motion of the ions is negligible. To a good approximation, the x-ray pulse creates a narrow cylindrical volume of electrons and nitrogen ions, and the electron cylinder broadens after the pulse has passed. At low pressures, the stopping of the electrons by the nitrogen is relatively weak, and the electrons would collide with the chamber walls without electric or magnetic fields.

A weak axial magnetic field can prevent electrons from hitting the wall, or at least slow down that process, given that the cyclotron radius $r = \upsilon m/qB$ is smaller than half the chamber radius. For photon energies of 0.83, 2.7, and 8.3 keV, this corresponds to magnetic fields of 35, 88, and 154 G, respectively.

Another process affecting the transport of electrons is space charge [8]. The photoelectrons and Auger electrons are ejected from the center of the chamber and leave positively charged ions behind and may eventually be electrostatically confined. In a simple model, we can describe the ions by a homogeneously charged cylinder of

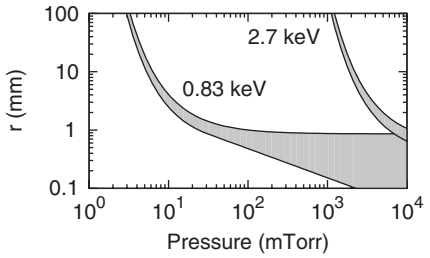

FIG. 3. Calculated travel distance of photoelectrons. For 8.3 keV, r is much larger than 100 mm.

radius R that is surrounded by a sheet of neutralizing electrons. Taking the cylinder radius as the x-ray beam FWHM, we estimate the distance that a photoelectron may travel. As mentioned above, the FWHM spot sizes are approximately 600 and 400 μm at 0.83 and 2.7 keV, respectively. Figure 3 shows r for $E_{\text{x-ray}} = 0.83$ and 2.6 keV as a function of the nitrogen pressure for a pulse energy of 1.5 mJ. The finite width of the curves represents the uncertainty of the spatial position of the primary electron. At 2.6 and 8.3 keV, space-charge effects are not expected to be significant for the photoelectrons. At 0.83 keV, space-charge effects are clearly present.

Figure 4 shows the time-integrated UV fluorescence signal as a function of the magnetic field for different photon energies and nitrogen pressures. For constant pressure, the signal is significantly lower for larger photon energies since the photon absorption cross section decreases, leading to fewer electrons emitted in total, i.e., fewer interaction with nitrogen molecules. The fluorescence signal increases with nitrogen pressure since more photons are absorbed and the primary electrons have more opportunities to deposit their energy into the gas since the mean-free path becomes smaller. Eventually, the electron energy deposition process saturates for large pressures. The signal also increases with increasing magnetic field since the primary electrons spend more time in the gas before colliding with the chamber walls, leading to an increased fraction of energy deposited into the nitrogen gas. This process saturates once the magnetic field is strong enough to confine the primary electrons to the gas.

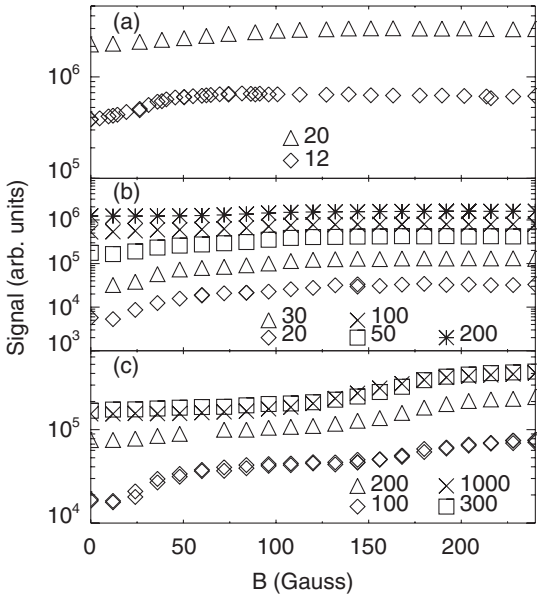

FIG. 4. Time-integrated fluorescence signal as a function of the magnetic field for photon energies of (a) 0.83 keV, (b) 2.7 keV, and (c) 8.3 keV. For each photon energy, data for different nitrogen pressures (given in mTorr) are shown.

Figure 5 shows the fluorescence signal duration (t_{FWHM}) as a function of the N_2 pressure for three photon energies at a magnetic field of 100 G. The signal duration is generally longer than the molecular fluorescent decay time of 20-30 ns, indicating that electron dynamics play an important role. A quantitative analysis would require a detailed model including electron-molecule collisions, electric and magnetic fields, and 3D geometry including wall effects. Such a study is also required to operate the detector without cross-calibration with another detection device and will be developed in future work. At present, we give a qualitative discussion of the main trends of the signal duration.

The dominant trend of decreasing signal duration with increasing pressure seen in Fig. 5 results from the decrease in collisional cascade times. The longest signal durations were observed at 0.83 keV. They decrease from 630 to 300 ns as the pressure is increased from 12 to 20 mTorr. The primary energy-loss mechanism for electrons with kinetic energies above 30 eV is electron impact ionization [9]. Since an electron loses around 40 eV in each event [5], a 420 eV photoelectron can undergo up to 10 inelastic collisions, given that it stays in the gas for a sufficiently long time. The Auger electrons have about the same energy and behave similarly. Although the mean-free paths of 400 eV electrons are in the range 10–16 cm, larger than the vessel radius, strong electrostatic confinement of the 400 eV electrons prevent them from colliding with the chamber walls (see Fig. 3). Therefore they will complete the ionization cascade within the N_2 gas. Using electron impact ionization cross sections [9], we estimate the time for the 400 eV electrons to reach 20–45 eV to be 250–610 ns and

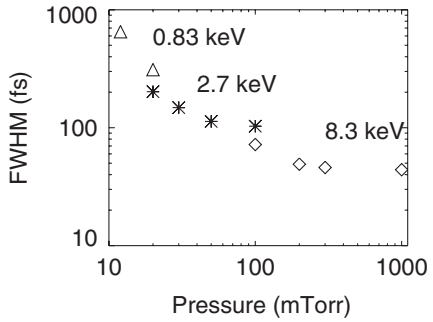

FIG. 5. Temporal width of the fluorescence signal as a function of the nitrogen pressure for different photon energies at a magnetic field of 100 G.

150–370 ns for 12 and 20 mTorr, respectively. These time scales are similar to the observed signal durations in Fig. 5, and demonstrate the decrease in duration with pressure. We note that electrostatic confinement effect may lead to a nonlinear dependence of the fluorescence signal on the pulse energy since space-charge effects are less pronounced at lower pulse energies, and the photoelectrons may not be able to deposit their full energy into the gas.

The signals are shorter for photon energies of 2.7 and 8.3 keV. For these energies, the relative contributions of photoelectrons and Auger electrons play a role. We examine this trend by comparing the results at 8.3 keV to those at 0.83 keV. At 8.3 keV space charge is not important. The collisional mean-free path of a photoelectron is 10 cm at 200 mTorr, so that it typically undergoes a single inelastic collision, if any, before colliding with the chamber wall after about 3 ns. Even at 1000 mTorr, photoelectrons undergo only 4 collisions, losing about 100 eV energy in the gas. However, the 420 eV Auger electrons deposit a significant amount of their energy into the gas, so that the 8.3 keV photon case is dominated by the dynamics of the Auger electrons. The stopping time for Auger electrons is estimated to be less than 60 ns, which is comparable to the signal duration seen in Fig. 5, and much shorter than the 0.83 keV results at lower pressure. As at 0.83 keV the pulse durations at 8.3 keV decrease with pressure, but this trend saturates as the internal molecular quenching time comes into play. Finally, at 2.7 keV, both photoelectrons and Auger electrons contribute to the fluorescence signal. The photoelectrons are not confined by space charge, but the Auger electrons are, depending on the pressure. In this case, the signal durations are intermediate between the low and high energy cases and we still see the decrease with pressure.

We have also measured the variation of signal duration with magnetic field. The major trend is an increase in duration with increasing magnetic field, resulting from increased confinement of the electrons in the gas. The variation is strongest at lower pressures and higher photon energies. For example, at 8.3 keV and 200 mTorr, the duration increases by 40% when the field is increased from 0 to 275 G.

In summary, we explored the interaction of high-intensity XFEL photon pulses between 0.83 and 8.3 keV with a nitrogen gas using UV fluorescence. Rough estimates for x-ray absorption, electron dynamics, and nitrogen fluorescence show that we can qualitatively understand the dependence of the UV fluorescence signal as a function of time, pressure, and magnetic field at 0.83 and 8.3 keV by considering the trajectories and stopping of the photoelectrons and Auger electrons in the nitrogen gas. For x-ray photon energies around 0.83 keV, space-charge confinement effects are significant, leading to the slowing and trapping of energetic electrons. Our results give confidence in the validity of models put forward to describe the interaction of XFEL radiation with matter [10], which are ultimately being used to understand experiments performed at XFELs. These results further find direct application for providing a sensitive *in situ*, nondestructive measurement of the XFEL pulse energy [3]. We have been able to validate the concept of such a gas detector, and identified regimes in which the fluorescence signal is expected to be linear in the XFEL pulse energy. At 8.3 keV, the gas detector is expected to be linear in the full operational pressure range of 100–1000 mTorr. At 0.83 keV the fluorescence emission is strongly influenced by the space-charge effects, and the gas detectors may become nonlinear: At very low pulse energies (and pressures), not much space charge is created, and the photoelectrons will escape from the interaction region and not deposit their full energy into the gas. At larger pulse energies (and pressures), all the energy of the photoelectrons is deposited in the nitrogen gas. If the gas detector is operated over a pulse energy range where it comes to a change in this trapping behavior, the fluorescence signal is not proportional to the pulse energy. The nonlinearity of the detector can be avoided by operating it only in a single regime, e.g., at very low pressures so that electrostatic confinement does not occur, or at very high pressures for which electrostatic confinement is present for any relevant pulse energies. An external magnetic field further ameliorates this problem. Further experiments at lower pulse energies will be required to verify this behavior.

This work performed under the auspices of the U.S. Department of Energy by Lawrence Livermore National Laboratory under Contract No. DE-AC52-07NA27344. B. Z. thanks G. Brenner, P. Juranic, and S. Toleikis for discussions.

[1] J. Arthur *et al.*, LCLS Conceptual Design Report No. SLAC-R-593, 2002.
[2] Y. Ding *et al.*, Phys. Rev. Lett. **102**, 254801 (2009).
[3] S. P. Hau-Riege, R. M. Bionta, D. D. Ryutov, and J. Krzywinski, J. Appl. Phys. **103**, 053306 (2008).
[4] B. L. Henke, E. M. Gullikson, and J. C. Davis, At. Data Nucl. Data Tables **54**, 181 (1993).
[5] S. P. Khare and A. Kumar, Jr., J. Phys. B **10**, 2239 (1977).
[6] A. Lofthus and P. H. Krupenie, J. Phys. Chem. Ref. Data **6**, 113 (1977).
[7] M. Nagano, K. Kobayakawa, N. Sakaki, and K. Ando, Astropart. Phys. **20**, 293 (2003).
[8] D. D. Ryutov, S. Hau-Riege, and R. M. Bionta, LLNL Report No. UCRL-TR-234930, SLAC Report No. LCLS-TN-07-11, 2007.
[9] Y. Itikawa, J. Phys. Chem. Ref. Data **35**, 31 (2006).
[10] B. Ziaja, R. A. London, and J. Hajdu, J. Appl. Phys. **99**, 033514 (2006).